Hemodynamic-Driven Multi-Prototypes Learning for One-Shot Segmentation in Breast Cancer DCE-MRI

Xiang Pan[1,2], Shiyun Nie[1], Tianxu Lv[1], and Lihua Li[3(✉)]

[1] School of Artificial Intelligence and Computer Science, Jiangnan University, Wuxi 214122, China
[2] Engineering Research Center of Intelligent Technology for Healthcare, Ministry of Education, Wuxi, China
[3] Institute of Biomedical Engineering and Instrumentation, Hangzhou Dianzi University, Hangzhou, China
lilh@hdu.edu.cn

Abstract. In dynamic contrast-enhanced magnetic resonance imaging (DCE-MRI) of the breast, tumor segmentation is pivotal in screening and prognostic evaluation. However, automated segmentation is typically limited by a large amount of fully annotated data, and the multi-connected regions and complicated contours of tumors also pose a significant challenge. Existing few-shot segmentation methods tend to overfit the targets of base categories, resulting in inaccurate segmentation boundaries. In this work, we propose a hemodynamic-driven multi-prototypes network (HDMPNet) for one-shot segmentation that generates high-quality segmentation maps even for tumors of variable size, appearance, and shape. Specifically, a parameter-free module, called adaptive superpixel clustering (ASC), is designed to extract multi-prototypes by aggregating similar feature vectors for the multi-connected regions. Moreover, we develop a cross-fusion decoder (CFD) for optimizing boundary segmentation, which involves reweighting and aggregating support and query features. Besides, a bidirectional Gate Recurrent Unit is employed to acquire pharmacokinetic knowledge, subsequently driving the ASC and CFD modules. Experiments on two public breast cancer datasets show that our method yields higher segmentation performance than the existing state-of-the-art methods. The source code will be available on https://github.com/Medical-AI-Lab-of-JNU/HDMP.

Keywords: One-Shot Segmentation · Breast Cancer segmentation · DCE-MRI · Superpixel Segmentation

1 Introduction

Semantic segmentation is pivotal in Computer-Aided Diagnosis (CAD) and various clinical applications such as diagnosis and surgical navigation. Typically, developing robust segmentation models relies on extensive image datasets annotated at the pixel level, posing a significant challenge for specific medical applications. Additionally, traditional semantic segmentation models may necessitate

partial retraining when faced with new clinical tasks. Few-Shot Segmentation (FSS) offers a novel approach to tackle these challenges. In recent years, few-shot segmentation (FSS) [10,15] has demonstrated promising performance in natural images but remains nascent in medical images. Therefore, our work primarily focuses on one-shot segmentation tasks with breast cancer data.

Dynamic contrast-enhanced magnetic resonance imaging (DCE-MRI) is extensively applied for discerning molecular subtypes of breast cancer [4,12], a pivotal consideration in clinical tasks such as surgical interventions. Breast cancer exhibits heterogeneity both morphologically and at the molecular level, requiring tailored treatment strategies for patients with distinct molecular subtypes. Recently, some methods [17, 23] have achieved particular success in breast cancer segmentation, but they fall short in discriminating between the subtypes of breast cancer. Therefore, accurately distinguishing molecular subtypes is also crucial for clinical tasks related to breast cancer.

Due to the high heterogeneity of breast tumors, resulting in variability in size, appearance, and shape, tumors exhibit features of multi-connected regions and complicated contours. We refer to the segmentation problem involving multi-connected regions and complicated contours as discrete region segmentation. Previous studies [3, 6] of few-shot medical image segmentation focus primarily on contiguous regions, achieving particular effectiveness in handling continuous regions. However, tackling the segmentation of discrete tumor regions remains an exceptionally formidable task. In previous few-shot prototype learning networks [20, 22], researchers commonly use mask average pooling to generate a single prototype for the foreground. Considering the multi-regional tumor modules in breast cancer, we have an insightful idea to cluster different regions into distinct prototypes, thereby providing a more detailed representation of object features. Additionally, in previous few-shot medical image segmentation studies [11, 16], inaccurate segmentation boundaries have posed a significant challenge as they solely depend on query features during decoding, disregarding the utilization of support features. We contend that harnessing support features can markedly improve segmentation results.

We propose a novel one-shot breast cancer segmentation approach in response to the abovementioned challenges. Leveraging a lightweight encoder-decoder architecture, we initially utilize a bidirectional Gate Recurrent Unit (GRU) [2] to acquire pharmacokinetic knowledge. Subsequently, we cluster discrete tumor regions and guide the pixel-wise allocation of query features. Finally, we introduce a distinctive decoder featuring the coexistence feature extractor as its core, aiming to capture the coexistence characteristics between support and query, thereby enhancing the accuracy of boundary segmentation. In summary, the primary contributions of this study are as follows: 1) We propose a hemodynamic-driven multi-prototypes network (HDMPNet) for one-shot segmentation, capable of generating high-quality segmentation maps even for discrete regions of breast cancer tumors. 2) We present the Adaptive Superpixel Clustering (ASC), a parameter-free module for adaptive prototype extraction with allocation, functioning as a plug-and-play component. 3) We propose a cross-fusion decoder

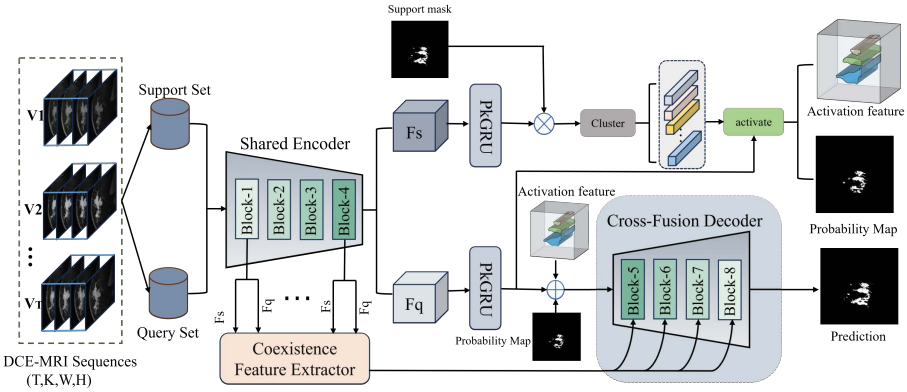

Fig. 1. Overview of the proposed Hemodynamic-Driven Multi-Prototypes Learning.

(CFD) that captures the coexistence characteristics between support and query, refining the segmentation boundaries with increased precision. 4) Compared to existing methods, our approach outperforms. Moreover, in external testing on another dataset, it achieves optimal segmentation.

2 Method

The proposed model, illustrated in Fig. 1, is tailored for breast cancer data analysis. Here, $\{V_t, t = 1, 2, \ldots, T\}$ represents a volumetric sequence of breast cancer-enhanced magnetic resonance imaging, spanning from the pre-contrast stage (t=1) to the post-contrast late stage (t=T). Concurrently, $V_t = \{S_D^t, D = 1,2,3, ..., K\}$ denotes a set of three-dimensional consecutive slices of breast volume, with K indicating the number of slices, and t representing a specific moment in pharmacokinetics. In our proposed model, we employ a shared encoder for feature extraction. Subsequently, we use pharmacokinetic modeling with the gate recurrent unit (PkGRU) to learn pharmacokinetic knowledge. Following this, clustering is applied to the support feature, generating multiple prototypes. The query feature is then activated to produce a corresponding activate feature and probability map. After that, we fuse the query features and support features through the Cross-Fusion Decoder (CFD) to achieve segmentation results.

2.1 Pharmacokinetic Modeling with Gate Recurrent Unit

In the pharmacokinetic modeling branch, we employ PkGRU to model the information from several temporal sequences of MRI images. Specifically, as illustrated in Fig. 2(a), PkGRU operates bidirectionally, capturing both forward and backward information to learn comprehensive features. These features are sequentially fed into the forward GRU module first and later into the backward

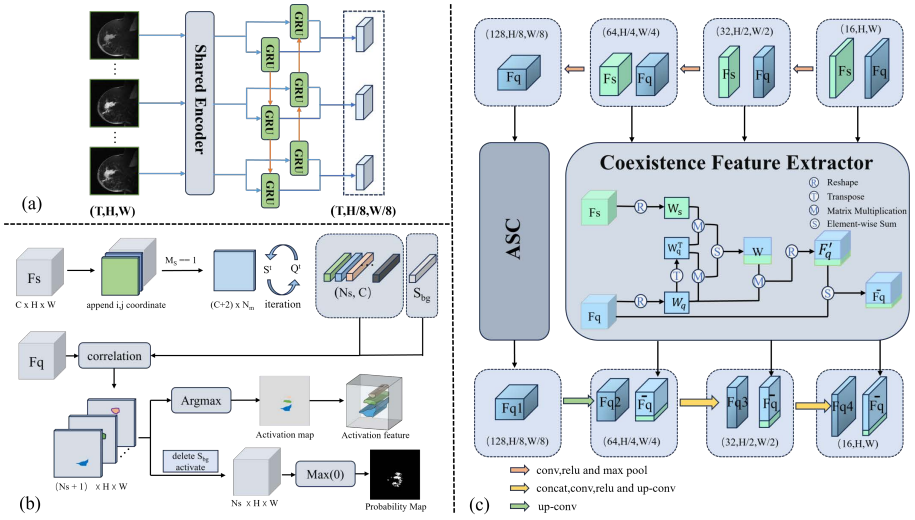

Fig. 2. Elaboration diagram of different component modules: (a) PkGRU, (b) ASC, and (c) CFD.

GRU module. Each GRU calculates update gates z_t and reset gates r_t, where x_t and the previous hidden state h_{t-1} are employed for storing updates, as follows:

$$z_t = \sigma(W_z x_t + V_z h_{t-1}), \quad r_t = \sigma(W_r x_t + V_r h_{t-1}) \tag{1}$$

Where σ denotes the sigmoid function. W_z, V_z, W_r and V_r are the learned weight matrices. Subsequently, the hidden state h_t is updated based on the gate controllers z_t and r_t. Formally,

$$\widehat{h_t} = \tanh\left(W x_t + r_t V h_{t-1} + \mathrm{b}\right), \quad h_t = (1 - z_t) h_{t-1} + z_t \widehat{h_t} \tag{2}$$

Where $\widehat{h_t}$ is denoted as the candidate hidden state, and b represents the bias vector. Next, we concatenate the results obtained from the forward GRU model h_t^f and the backward GRU model h_t^b to form the final result $h_t^B i$.

2.2 Adaptive Superpixel Clustering

Inspired by SSN [8] and MaskSLIC [7], and acknowledging the challenge posed by tumor discreteness, we propose an insightful approach: clustering tumor regions into multiple superpixel centroids, treating each superpixel centroid as a prototype. First, we input the support features $F_s \in \mathbb{R}^{c \times h \times w}$, support mask $M_s \in \mathbb{R}^{h \times w}$ and initial superpixel seeds $S^0 \in \mathbb{R}^{c \times N_s}$ (where N_s represents the number of superpixels), with S^0 setting referenced from MaskSLIC [7]. We transform the support feature, retaining only foreground information, resulting in $F_s' \in \mathbb{R}^{c \times N_{pm}}$ (where N_{pm} is the number of pixels in the support mask). Following this, we engage in an iterative process, updating each superpixel centroid

and redistributing each pixel accordingly:

$$Q_{pi}^{t} = e^{-\left\|F_{p}^{\prime} - S_{i}^{t-1}\right\|^{2}}, \quad S_{i}^{t} = \frac{1}{Z_{i}^{t}} \sum_{p=1}^{N_{p}m} Q_{pi}^{t} F_{i}^{\prime} \tag{3}$$

Where $||\cdot||^2$ represents the distance calculation between two vectors. Q_{pi}^{t} represents the association between each pixel p and each superpixel centroid at time t. S_{i}^{t} denotes the update of each superpixel centroid, where $Z_{i}^{t} = \Sigma_{p} Q_{pi}^{t}$ is the normalization constant.

Next, we utilize masked average pooling to distill background information into an additional prototype, subsequently merging it with the foreground prototype. Next, we compute the affinity between the query feature Fq at each spatial position and each prototype. Mathematically, this can be expressed as:

$$\mathbf{A}_{i}^{x,y} = g_{\varphi}(\mathbf{F}_{\mathbf{q}}^{\mathbf{x},\mathbf{y}} \oplus S_{\mathrm{a}}^{i}) \quad i \in \{1, 2, \ldots, N_{s} + 1\} \tag{4}$$

Where S_{a}^{i} denotes the i-th prototype, and $\oplus$ represents channel-wise concatenation. The function $g_{\varphi}(\cdot)$ is utilized to compute the correlation between two vectors. We employ three 1 x 1 convolutions, followed by a sigmoid activation function to formulate $g_{\varphi}(\cdot)$.

Next, our architecture comprises two branches. In the first branch, we employ argmax to determine the index with the highest score for each spatial position, yielding an activation map $M \in \mathbb{R}^{1 \times h \times w}$. Subsequently, placing the corresponding prototype at each position of the activation map yields activation feature $F_A \in \mathbb{R}^{c \times h \times w}$. In the second branch, we remove the feature channels activated by the background prototype and then apply a Max operation on the remaining channels to obtain the probability map P. As shown in Fig. 2(b).

Considering adaptability, we define the number of superpixels as N_s:

$$N_{s} = min(\left\lfloor \frac{N_{pm}}{S_{s}} \right\rfloor, N_{max}) \tag{5}$$

Where S_s is the average area of each initial superpixel seed, and N_{max} can be assigned differently based on various datasets.

2.3 Cross-Fusion Decoder

To address the challenge of inaccurate boundary segmentation, we build a Cross-Fusion Decoder (CFD). The entire decoding structure is similar to U-Net [19]. We design a coexistence feature extractor in each decoding layer to capture the coexistence features between the support and query. As illustrated in Fig. 2(c), we first reshape the support and query features $\mathbf{F_s}, \mathbf{F_q} \in \mathbb{R}^{c \times h \times w}$ into $\mathbf{W_s}, \mathbf{W_q} \in \mathbb{R}^{c \times N}$ respectively. Subsequently, we transpose $\mathbf{W_q}$ to obtain $\mathbf{W_q^T}$. We perform matrix multiplication operations separately for $\mathbf{W_s}$ and $\mathbf{W_q}$ followed by merging them together using a learnable parameter λ, which is formulated as:

$$\mathbf{W} = \mathbf{W_q} \mathbf{W_q^T} + \lambda \mathbf{W_s} \mathbf{W_q^T} \tag{6}$$

Where $\mathbf{W} \in \mathbb{R}^{c \times c}$ represents the channel-wise fusion weights. Next, we perform matrix multiplication for $\mathbf{W}$ and $\mathbf{W_q}$ to obtain $\mathbf{W}' \in \mathbb{R}^{c \times N}$, and then reshape it into $\mathbf{F'_q} \in \mathbb{R}^{c \times h \times w}$. Finally, a residual-like structure is adopted to reweight $\mathbf{F'_q}$ and $\mathbf{F_q}$ to obtain $\overline{\mathbf{F}_q}$.

3 Experiments

Dataset: We evaluate our method on two publicly available datasets. (1) The Breast-MRI-NACT-Pilot dataset [18] contains a total of 64 patients with the contrast-enhanced MRI protocol: a pre-contrast scan, followed by two consecutive post-contrast time points during the early and late phases. Molecular subtypes for each patient are recorded in an additional clinical information workbook. Inspired by Haibe-Kains *et al.* [5] and Li *et al.* [13], we categorize the data into four classes: Basal-like, HER2-enriched, Luminal, and Normal-like (benign tumor). (2) The Cancer Genome Atlas Breast Invasive Carcinoma Collection (TCGA-BRCA) [14] includes longitudinal DCE-MRI studies of 139 participants. We categorize the data according to the Breast-MRI-NACT-Pilot [18] typing criteria and the same four categories above. Both datasets are available on The Cancer Imaging Archive (TCIA).

Implementation Details: Our complete framework is implemented in PyTorch and trained on an NVIDIA GeForce RTX 4090. We conduct a 4-fold experiment on the Breast-MRI-NACT-Pilot dataset [18], designating one typing as an unknown semantic class once per-fold. Specifically, we select three typing categories during the training process, leaving one typing for testing. Notably, the semantic classes used for testing in the evaluation phase do not appear during training. For the three fully supervised methods, we conduct two types of experiments: one involves conducting independent experiments for each time series, while the other uses complete sequence. Finally, we select the best results (U-Net [19] performs best with the complete sequence, while TransUNet [1] and MSA [21] achieve their best results with the post-contrast late phase). For the three FFS methods, we utilize our proposed PkGRU for time series processing. We normalize all MRI scans to the range [0, 1] and utilize the Dice Similarity Coefficient (DSC) as the evaluation metric.

Comparison With Existing Methods: We compare our method against six approaches from two categories on the Breast-MRI-NACT-Pilot [18] breast dataset: Few-Shot Segmentation (FSS), including BiGRU [9], PFENet [20], and RAPNet [3], and fully supervised segmentation methods, including U-Net [19], TransUNet [1], and MSA [21]. For the FSS methods, we all use a one-shot experimental setup. Quantitative results are presented in Table 1, while Fig. 3 provides a visual representation of the segmentation outcomes. Our method demonstrates superior performance compared to other models, achieving an average Dice score of 67.9%, as shown in Table 1. We speculate that PFENet's poorer results may

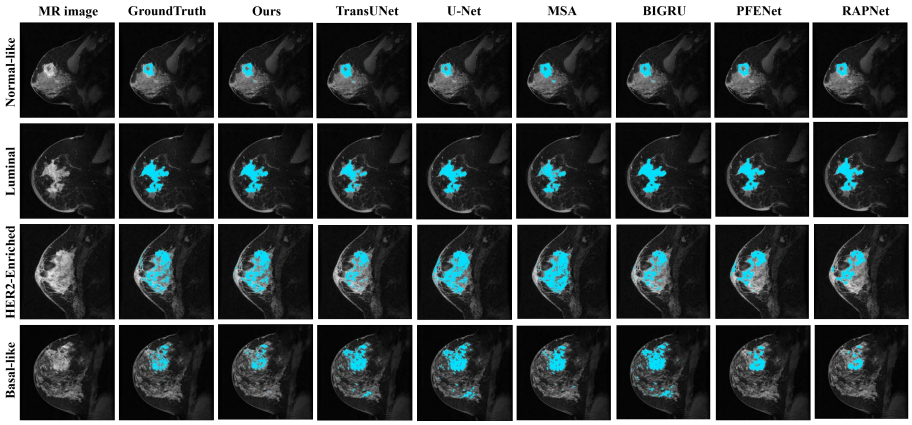

Fig. 3. Visual comparison of different segmentation methods.

Table 1. Quantitative Comparison (in Dice score %) of different methods on Breast-MRI-NACT-Pilot.

Method	Normal-like	Luminal	HER2-enriched	Basal-like	mean
U-Net [19]	55.1 ± 2.2	$\mathbf{76.5 \pm 2.5}$	66.0 ± 2.6	63.9 ± 2.8	65.4
TransUNet [1]	44.8 ± 2.8	54.6 ± 2.6	54.8 ± 3.2	50.7 ± 2.9	51.2
MSA [21]	42.7 ± 2.0	60.1 ± 2.1	50.4 ± 2.4	52.1 ± 2.5	51.3
BIGRU [9]	50.3 ± 1.8	69.1 ± 2.1	61.8 ± 2.2	59.4 ± 2.0	60.2
PFENet [20]	31.8 ± 2.9	52.5 ± 2.8	41.2 ± 2.7	40.9 ± 2.6	41.6
RAPNet [3]	30.7 ± 2.5	50.6 ± 2.9	40.2 ± 3.2	38.0 ± 2.2	39.9
Ours	$\mathbf{60.7 \pm 2.4}$	76.4 ± 2.0	$\mathbf{69.1 \pm 1.8}$	$\mathbf{65.4 \pm 3.1}$	**67.9**

stem from the domain gap between natural and medical images, as PFENet is designed for natural images. RAPNet's performance may be influenced by the similar location of foreground regions in the processed dataset. It may be attributed to the limited number of samples in the dataset, resulting in less than ideal performance of TransUNet and MSA.

Ablation Study: We conduct extensive ablation experiments on the Breast-MRI-NACT-Pilot dataset [18] to validate the effectiveness of the critical components of our model. Our baseline utilizes single prototype learning proposed in PFENet [20]. For 4D data, we directly concatenate temporal sequence information through channel stacking and employ a lightweight encoder-decoder structure. The experimental results in Table 2 demonstrate the effectiveness of our model components. Replacing the single prototype in the baseline with our ASC module yields an average DSC improvement of 3.2%. We speculate that using a single prototype to represent all category information may lead to ambiguity, necessitating more refined feature information. The addition of the PkGRU module

Table 2. Ablation study of three component modules.

Experiments	Normal-like	Luminal	HER2-enriched	Basal-like	mean
baseline	49.5 ± 2.0	67.7 ± 2.1	59.8 ± 2.1	57.6 ± 2.2	58.7
baseline+ASC	51.1 ± 1.8	70.2 ± 2.2	63.9 ± 2.2	62.2 ± 2.0	61.9
baseline+ASC+CFD	56.5 ± 2.0	74.5 ± 2.2	67.2 ± 2.1	64.3 ± 2.2	65.6
baseline+ASC+PkGRU	53.2 ± 1.9	72.3 ± 2.1	65.1 ± 2.0	63.8 ± 2.1	63.6
baseline+ASC+PkGRU+CFD	$\mathbf{60.7 \pm 2.4}$	$\mathbf{76.4 \pm 2.0}$	$\mathbf{69.1 \pm 1.8}$	$\mathbf{65.4 \pm 3.1}$	**67.9**

Table 3. External testing results of different methods on TCGA-BRCA(Dice score %).

External test	Normal-like	Luminal	HER2-enriched	Basal-like	mean
U-Net [19]	60.2 ± 1.8	72.0 ± 2.2	83.0 ± 2.3	81.6 ± 2.5	74.2
TransUNet [1]	$\mathbf{76.0 \pm 2.2}$	71.1 ± 2.4	70.0 ± 2.8	79.4 ± 2.9	74.1
MSA [21]	68.4 ± 2.6	73.7 ± 2.4	83.9 ± 2.5	79.7 ± 2.4	76.4
BIGRU [9]	60.2 ± 2.5	66.2 ± 2.2	70.5 ± 2.8	68.1 ± 2.8	66.3
PFENet [20]	58.9 ± 2.5	61.1 ± 2.5	65.5 ± 2.5	64.8 ± 2.0	62.6
RAPNet [3]	48.9 ± 2.2	52.3 ± 2.5	55.1 ± 2.8	53.6 ± 2.2	52.5
Ours	64.0 ± 2.5	$\mathbf{75.3 \pm 2.8}$	$\mathbf{87.7 \pm 2.8}$	$\mathbf{82.2 \pm 2.4}$	**77.3**

increases the average DSC by 1.75%, potentially due to the limitation of channel stacking in capturing pharmacokinetic knowledge. Subsequently, integrating the CFD module enhances the average DSC by 3.775%. We attribute this improvement to the comprehensive utilization of support features by CFD, extracting coexistence characteristics between support and query data, and refining local features of boundaries, which facilitates more effective decoding.

External test: MRI images may exhibit diversity due to variations in acquisition equipment, parameter settings, and data sources. This diversity can potentially impact the performance of deep learning models, necessitating continual fine-tuning or even retraining on new datasets. We train our model using three subtypes of data from the Breast-MRI-NACT-Pilot dataset [18] and test it on the fourth subtype from TCGA-BRCA [14]. Experimental results, as depicted in Table 3, demonstrate that our approach achieves optimal performance, with an average DSC of 77.3%. This achievement holds significant clinical relevance in real-world applications and underscores the strong generalization capabilities of our model.

4 Conclusion

We propose a novel one-shot segmentation method that leverages pharmacokinetic knowledge for clustering and guiding prototype allocation. This approach

incorporates a decoder integrating support and query data, producing high-quality segmentation results. Our method yields promising outcomes even for breast cancer data with discrete tumor area samples. Additionally, during external testing, our model adapts to new clinical tasks with just one label, addressing challenges associated with limited annotated data in clinical settings. This approach holds significant potential for future applications.

Acknowledgments. This work is supported in part by the National Key R&D Program of China under Grants 2018YFA0701700 and 2021YFE0203700, the Postgraduate Research & Practice Innovation Program of Jiangsu Province SJCX22_1106, and is supported by National Natural Science Foundation of China grants U21A20521 and 62271178, Zhejiang Provincial Natural Science Foundation of China (LR23F010002), Jiangsu Provincial Maternal and Child Health Research Project (F202034), Wuxi Health Commission Precision Medicine Project (J202106), Jiangsu Provincial Six Talent Peaks Project (YY-124), and the construction project of Shanghai Key Laboratory of Molecular Imaging (18DZ2260400).

Disclosure of Interests. The authors have no competing interests to declare that are relevant to the content of this article.

References

1. Chen, J., Lu, Y., Yu, Q., Luo, X., Adeli, E., Wang, Y., Lu, L., Yuille, A.L., Zhou, Y.: Transunet: Transformers make strong encoders for medical image segmentation. arXiv preprint arXiv:2102.04306 (2021)
2. Cho, K., Van Merriënboer, B., Gulcehre, C., Bahdanau, D., Bougares, F., Schwenk, H., Bengio, Y.: Learning phrase representations using rnn encoder-decoder for statistical machine translation. arXiv preprint arXiv:1406.1078 (2014)
3. Feng, Y., Wang, Y., Li, H., Qu, M., Yang, J.: Learning what and where to segment: A new perspective on medical image few-shot segmentation. Medical Image Analysis **87**, 102834 (2023)
4. Haibe-Kains, B., Desmedt, C., Loi, S., Culhane, A.C., Bontempi, G., Quackenbush, J., Sotiriou, C.: A three-gene model to robustly identify breast cancer molecular subtypes. Journal of the National Cancer Institute **104**(4), 311–325 (2012)
5. Haibe-Kains, B., Desmedt, C., Loi, S., Culhane, A.C., Bontempi, G., Quackenbush, J., Sotiriou, C.: A three-gene model to robustly identify breast cancer molecular subtypes. Journal of the National Cancer Institute **104**(4), 311–325 (2012)
6. Hansen, S., Gautam, S., Jenssen, R., Kampffmeyer, M.: Anomaly detection-inspired few-shot medical image segmentation through self-supervision with supervoxels. Medical Image Analysis **78**, 102385 (2022)
7. Irving, B.: maskslic: regional superpixel generation with application to local pathology characterisation in medical images. arXiv preprint arXiv:1606.09518 (2016)
8. Jampani, V., Sun, D., Liu, M.Y., Yang, M.H., Kautz, J.: Superpixel sampling networks. In: Proceedings of the European Conference on Computer Vision (ECCV). pp. 352–368 (2018)
9. Kim, S., An, S., Chikontwe, P., Park, S.H.: Bidirectional rnn-based few shot learning for 3d medical image segmentation. In: Proceedings of the AAAI conference on artificial intelligence. vol. 35, pp. 1808–1816 (2021), https://ojs.aaai.org/index.php/AAAI/article/view/16275

10. Lang, C., Cheng, G., Tu, B., Li, C., Han, J.: Base and meta: A new perspective on few-shot segmentation. IEEE Transactions on Pattern Analysis and Machine Intelligence (2023)
11. Lei, W., Su, Q., Jiang, T., Gu, R., Wang, N., Liu, X., Wang, G., Zhang, X., Zhang, S.: One-shot weakly-supervised segmentation in 3d medical images. IEEE Transactions on Medical Imaging (2023)
12. Li, H., Zhu, Y., Burnside, E.S., Huang, E., Drukker, K., Hoadley, K.A., Fan, C., Conzen, S.D., Zuley, M., Net, J.M., et al.: Quantitative mri radiomics in the prediction of molecular classifications of breast cancer subtypes in the tcga/tcia data set. NPJ breast cancer **2**, 16012 (2016)
13. Li, H., Zhu, Y., Burnside, E.S., Huang, E., Drukker, K., Hoadley, K.A., Fan, C., Conzen, S.D., Zuley, M., Net, J.M., et al.: Quantitative mri radiomics in the prediction of molecular classifications of breast cancer subtypes in the tcga/tcia data set. NPJ breast cancer **2**, 16012 (2016)
14. Lingle, W., et al.: The cancer genome atlas breast invasive carcinoma collection (tcga-brca)(version 3)[data set]. cancer imag. arch.(2016)
15. Liu, W., Zhang, C., Lin, G., Liu, F.: Crcnet: Few-shot segmentation with cross-reference and region–global conditional networks. International Journal of Computer Vision **130**(12), 3140–3157 (2022)
16. Lu, Y., Zheng, K., Li, W., Wang, Y., Harrison, A.P., Lin, C., Wang, S., Xiao, J., Lu, L., Kuo, C.F., et al.: Contour transformer network for one-shot segmentation of anatomical structures. IEEE transactions on medical imaging **40**(10), 2672–2684 (2020)
17. Lv, T., Liu, Y., Miao, K., Li, L., Pan, X.: Diffusion kinetic model for breast cancer segmentation in incomplete dce-mri. In: International Conference on Medical Image Computing and Computer-Assisted Intervention. pp. 100–109. Springer (2023), https://doi.org/10.1007/978-3-031-43901-8_10
18. Newitt, D., Hylton, N.: Single site breast dce-mri data and segmentations from patients undergoing neoadjuvant chemotherapy. The Cancer Imaging Archive **2** (2016)
19. Ronneberger, O., Fischer, P., Brox, T.: U-net: Convolutional networks for biomedical image segmentation. In: Medical Image Computing and Computer-Assisted Intervention–MICCAI 2015: 18th International Conference, Munich, Germany, October 5-9, 2015, Proceedings, Part III 18. pp. 234–241. Springer (2015), http://dx.doi.org/10.1007/978-3-319-24574-4_28
20. Tian, Z., Zhao, H., Shu, M., Yang, Z., Li, R., Jia, J.: Prior guided feature enrichment network for few-shot segmentation. IEEE transactions on pattern analysis and machine intelligence **44**(2), 1050–1065 (2020)
21. Wu, J., Fu, R., Fang, H., Liu, Y., Wang, Z., Xu, Y., Jin, Y., Arbel, T.: Medical sam adapter: Adapting segment anything model for medical image segmentation. arXiv preprint arXiv:2304.12620 (2023)
22. Zhang, C., Lin, G., Liu, F., Yao, R., Shen, C.: Canet: Class-agnostic segmentation networks with iterative refinement and attentive few-shot learning. In: Proceedings of the IEEE/CVF conference on computer vision and pattern recognition. pp. 5217–5226 (2019)
23. Zhong, Y., Wang, Y.: Simple: Similarity-aware propagation learning for weakly-supervised breast cancer segmentation in dce-mri. In: International Conference on Medical Image Computing and Computer-Assisted Intervention. pp. 567–577. Springer (2023), https://doi.org/10.1007/978-3-031-43901-8_54